First-principles calculation of phase equilibrium of V-Nb, V-Ta, and Nb-Ta alloys

C. Ravi,* B. K. Panigrahi, and M. C. Valsakumar
Materials Science Group, Indira Gandhi Center for Atomic Research, Kalpakkam 603 102, Tamil Nadu, India

Axel van de Walle
Engineering and Applied Sciences Division, California Institute of Technology, Pasadena, California 91125, USA
(Received 15 November 2011; published 7 February 2012)

In this paper, we report the calculated phase diagrams of V-Nb, V-Ta, and Nb-Ta alloys computed by combining the total energies of 40–50 configurations for each system (obtained using density functional theory) with the cluster expansion and Monte Carlo techniques. For V-Nb alloys, the phase diagram computed with conventional cluster expansion shows a miscibility gap with consolute temperature $T_c = 1250$ K. Including the constituent strain to the cluster expansion Hamiltonian does not alter the consolute temperature significantly, although it appears to influence the solubility of V- and Nb-rich alloys. The phonon contribution to the free energy lowers T_c to 950 K (about 25%). Our calculations thus predicts an appreciable miscibility gap for V-Nb alloys. For bcc V-Ta alloy, this calculation predicts a miscibility gap with $T_c = 1100$ K. For this alloy, both the constituent strain and phonon contributions are found to be significant. The constituent strain increases the miscibility gap while the phonon entropy counteracts the effect of the constituent strain. In V-Ta alloys, an ordering transition occurs at 1583 K from bcc solid solution phase to the V_2Ta Laves phase due to the dominant chemical interaction associated with the relatively large electronegativity difference. Since the current cluster expansion ignores the V_2Ta phase, the associated chemical interaction appears to manifest in making the solid solution phase remain stable down to 1100 K. For the size-matched Nb-Ta alloys, our calculation predicts complete miscibility in agreement with experiment.

DOI: 10.1103/PhysRevB.85.054202 PACS number(s): 64.75.−g, 61.66.−f

I. INTRODUCTION

Vanadium, niobium, tantalum, and their binary alloys have been the subject of research due to their superconducting properties and low-temperature structural phase transformations.[1–5] Short-range order and superconductivity of V-Nb, V-Ta, and Nb-Ta alloys have been examined for understanding the influence of alloying on the superconducting transition temperatures.[2] Recently, V, Nb, and Ta have been found to undergo a martensitic-like structural distortion [3–5] in which they transform from the high-temperature bcc structure to either a rhombohedral structure or to a tetragonal structure. Apart from this, vanadium-based alloys are known to have the desired combination of physicomechanical properties, compatibility with nuclear fuel, and high resistance to corrosion [6,7] making them potential structural materials for fast-neutron nuclear power plants which can be operated at temperatures exceeding 1000 K for increasing the thermodynamic efficiency of electric power production.

The capability of vanadium to form a continuous series of solid solutions with other refractory metals makes it possible to design binary, ternary, and more complex alloys based on it. Alloying is found to significantly increase the resistance to creep and deformation of vanadium. Nb, Ta, and W are found to harden vanadium significantly compared to Ti, Zr, and Cr. In V-Nb-Zr-C alloy, the high-temperature strength increases markedly with increasing Nb concentration. On the other hand, it is known that the state of atomic order of the alloy determines its hardness, strength, corrosion properties, and electrical resistivity. Decay of the solid solution to ordering or phase separation is known to significantly lower the hardness and resistance to corrosion of many alloys. In other words, the ordering or phase separation behavior of the alloy decides many physical properties, including microstructure, transport, and mechanical behavior. This means that knowledge of the alloy phase equilibrium and phase transformation properties is essential for effective design of the alloy.

The experimental phase diagram of V-Nb alloys shows a continuous series of solid solutions without a miscibility gap. The solid state part of the V-Ta phase diagram consists of a major solid solution region and a two-phase region made up of the V_2Ta Laves phase and bcc solid solution. The Nb-Ta phase diagram shows complete miscibility in the solid state without any evidence for a solid-state transformation down to ambient temperature.[8,9] Recent first-principles study of phase equilibrium of similar refractory bcc binary alloys, such as Nb-Mo, Nb-W, Ta-W, and Ta-Mo, has however predicted several intermediate ground states.[10] For V-Nb, V-Ta, and Nb-Ta systems, while there exist a few CALPHAD studies, first-principles studies of phase equilibrium do not exist in the literature.

This work aims to corroborate and complement these experimental observations by more precisely locating the position of the miscibility gap in these systems via first-principles calculations. Although both V-Nb and Nb-Ta were previously reported to exhibit complete solubility, we in fact find that their miscibility gaps have rather different locations (around 950 K for V-Nb but close to 0 K for Nb-Ta). This has important implications for thermodynamic modeling in these systems. Moreover, our analysis of the metastable bcc phase diagram of the V-Ta system avoids masking by the V_2Ta Laves phase and enables the determination of the bcc miscibility gap. Furthermore, calculation of phase stability of V-Nb alloys is also of interest because in the high-chromium ferritic-martensitic steels, considered as a substitute for austenitic steels in nuclear reactors, fine dispersions of two distinct vanadium nitrides, $V_{0.6}Nb_{0.2}Cr_{0.2}N$ and $V_{0.45}Nb_{0.45}Cr_{0.1}N$, are

known to precipitate and remain stable against coarsening leading to enhanced creep strength.[11–16] Experience in carrying out the phase equilibrium calculation of the binary systems studied here would be a valuable input for the study of phase stability of V-Nb(Cr)-N (qua)ternary nitrides.

We use density functional theory based total energy calculations combined with the cluster expansion and Monte Carlo techniques for calculation of phase equilibrium. Cluster expansion consists of considering the alloy being made of "geometric objects" (or figures), such as points, pairs, triplets, and associating a characteristic energy J with each of these geometric objects. For a given underlying Bravais lattice, cluster expansion then expresses the energy $E(\sigma)$ of any configuration σ of the alloy as a linear combination of the characteristic energies J and the correlation functions of every figure, like a generalized Ising Hamiltonian. Finite-temperature properties are calculated by resorting to Monte Carlo simulations using the cluster expansion Hamiltonian $E(\sigma)$. Furthermore, our cluster expansion Hamiltonian includes the strain energy due to lattice constant mismatch of the constituents and the phonon contributions besides chemical interactions, which are known to improve the accuracy of the computed thermodynamic properties.[17–32]

The paper is organized as follows: A brief review of the formalism of the cluster expansion method and Monte Carlo simulation is given in Sec. II. In Sec. III the results are presented. The results are discussed in Sec. IV, and our findings are summarized in the final section.

II. METHODOLOGY

A. Cluster expansion

Computation of phase equilibrium and ground-state structure of an $A_{1-x}B_x$ binary alloy requires, in principle, calculation of the total energy for all possible configurations of placing atoms A and B on N sites of the underlying Bravais lattice. As the number of possible configurations 2^N becomes enormous even for a modest number of sites N, it is difficult to calculate the energy quantum mechanically for an exhaustive set of configurations. The cluster expansion method constructs an Ising-like Hamiltonian for the energies of the different atomic configurations. Detailed illustration of the method can be found in many papers.[18,20,26,33–39] Here a brief description of the main aspects is given. In the cluster expansion, the alloy is treated as a lattice problem in which the lattice sites are fixed at those of the underlying Bravais lattice (fcc, bcc, etc.) and a configuration σ is defined by specifying the occupation of each of the N lattice sites by an A atom or a B atom. For each configuration, one assigns a set of "spin" variables $\hat{S}_i$ ($i = 1,2,\ldots,N$) to each of the N sites of the lattice, with $\hat{S}_i = -1$ or $+1$ depending on the site i being occupied by an A or B atom, respectively. For a lattice with N sites, the problem of calculating the energies of the 2^N possible configurations σ can be exactly mapped into a generalized Ising Hamiltonian:

$$E(\sigma) = J_0 + \sum_i J_i \hat{S}_i(\sigma) + \sum_{j<i} J_{ij} \hat{S}_i(\sigma)\hat{S}_j(\sigma) + \sum_{k<j<i} J_{ijk} \hat{S}_i(\sigma)\hat{S}_j(\sigma)\hat{S}_k(\sigma) + \cdots, \quad (1)$$

where the J's are the interaction energies of various order, also known as the effective cluster interactions. The first summation is over all sites in the lattice, the second over all pairs of sites, the third over all triplets, and so on. The primary advantage of the cluster expansion is that the J's are the same for all configurations σ. Thus, once the J's are known, the energy $E(\sigma)$ of any configuration can be calculated almost immediately by simply calculating the spin products and summing them using Eq. (1).

Equation (1) defines a set of linear equations, in which a $2^N \times 2^N$ matrix of spin products multiplies a 2^N vector of J's, giving a vector of the energies of the 2^N configurations. The J's can then be solved exactly if the matrix of spin products is nonsingular. Sanchez *et al.*[33] have proven that the matrix is indeed orthogonal which guarantees that the vector of J's in Eq. (1) can always be determined.

Although the cluster expansion given by Eq. (1) contains, in principle, many interactions, the energetics of bonding is usually determined by relatively short length scales. Therefore, a finite number of interaction parameters is expected to provide the desired mapping of energetics with sufficient accuracy. Then one can determine the J's from the energies of a small set of ordered configurations, calculated directly, for instance, by first-principles total-energy methods. Once numerical values for the parameters J are available, the payoff is fast access to many properties of interest, e.g., ground-state structures, order-disorder transition temperatures, short-range order, and composition-temperature phase diagrams, which can be directly determined by experiments.

The lattice symmetry further reduces the number of interaction energies that need to be determined. A set of lattice sites, called a "figure," has the same interaction energy as any other figure that is related to it by the space-group symmetry of the underlying lattice. A correlation function $\overline{\Pi}$ can be defined for each class of symmetry-equivalent figures F and configuration σ as the average of the spin products over all figures that make up F:

$$\overline{\Pi}_F(\sigma) = \frac{1}{M_F} \sum_f \hat{S}_{i_1}(\sigma)\hat{S}_{i_2}(\sigma)\ldots\hat{S}_{i_n}(\sigma), \quad (2)$$

where f runs over the M_F figures in class F, and the spin indices run over the n sites of figure f. Equation (1) can then be rewritten for the energy of formation of structure σ as

$$\Delta H_{\mathrm{CE}}(\sigma) = N \sum_F D_F J_F \overline{\Pi}_F(\sigma), \quad (3)$$

where D_F is the number of figures of class F per site. The important step of the cluster expansion method is the determination of the J's. In the direct inversion method of Connolly and Williams,[40] energy of formation of N_σ ($\approx$30–40) ordered configurations are calculated directly. N_F figures are chosen, with $N_F \leqslant N_\sigma$, such that the cluster expansion of Eq. (3) is converged when the sum is restricted to these N_F figures. The correlation functions, $\overline{\Pi}$, and the calculated energies of formation, $\Delta H_{\mathrm{direct}}(\sigma)$, of these configurations are

then used to fit the interaction energies J_F, by minimizing the following expression with respect to the N_F values of J_F:

$$\sum_{\sigma}^{N_\sigma} \omega_\sigma \left| \Delta H_{\text{direct}}(\sigma) - N \sum_{F}^{N_F} D_F J_F \overline{\Pi}_F(\sigma) \right|^2 . \quad (4)$$

Here ω_σ are weights. The weights are chosen according to $\omega_\sigma = g/N_c(\sigma)$, where $N_c(\sigma)$ is the number of point group operations of configuration σ and g is the order of the point group of the underlying Bravais lattice. The expression (4) is minimized typically using the singular value decomposition technique.

B. Density functional theory calculations

Electronic structure total energy calculations of ordered configurations, required for the construction of the cluster expansion Hamiltonian, are performed using the Vienna *Ab initio* Simulation Package[41,42] (VASP) with the generalized gradient approximation (GGA)[43–46] and the projector augmented wave (PAW) basis[47,48] with an energy cutoff of 400 eV. The first-order Methfessel-Paxton method[49] of electronic occupancy has been used with a smearing width of 0.2 eV. Brillouin zone integration is carried out using a Monkhorst-Pack k-point mesh.[50] For constructing the cluster expansion Hamiltonian and calculation of thermodynamic properties, the Alloy Theory Automated Toolkit (ATAT) has been used.[51–53] ATAT uses a script interface to VASP. This script defines a parameter called KPPRA, which automatically sets up the k-point mesh for similar systems. In this work KPPRA is set to 8000, which, for bcc V, translates to a $20 \times 20 \times 20$ grid. These choices of basis cutoff and k-point grid ensure convergence of the total energy within a few meV/atom.

C. Constituent strain energy

The conventional cluster expansion described above considers the chemical interactions and their configuration dependence. It ignores the strain energy due to the size mismatch of the constituent atoms. The constituent strain energy, defined as the energy required to maintain coherency along an interface between bulk crystals A and B, is however significant in general. It is required for the accurate calculation of phase diagrams, miscibility gap temperature, short-range order, etc.[18,22–25,37,54–57] V-Nb and V-Ta alloys have a lattice constant mismatch of 8.5%. Nb-Ta is a size-matched alloy. V-Nb and V-Ta alloys could be expected to show appreciable atomic relaxations. Therefore, the conventional cluster expansion of Eq. (3) has to be modified such that it accounts for both the chemical interactions and constituent strain energies, and produces accurate formation energy for any configuration σ with the atomically relaxed geometry and equilibrium volume. The modified expression for $\Delta H_{\text{CE}}(\sigma)$ is given below:

$$\Delta H_{\text{CE}}(\sigma) = N \sum_{F} D_F J_F \overline{\Pi}_F(\sigma) + \Delta E_{\text{CS}}(\sigma). \quad (5)$$

Here the first term is the conventional cluster expansion representing the chemical interactions and the second term is the strain energy due to lattice constant mismatch.

The strain energy $\Delta E_{\text{CS}}(\sigma)$ of configuration σ is expressed as

$$\Delta E_{\text{CS}}(\sigma) = \sum_{\mathbf{k}} J_{\text{CS}}(x,\hat{k}) |S(\mathbf{k},\sigma)|^2, \quad (6)$$

$$J_{\text{CS}}(x,\hat{k}) = \frac{\Delta E^{\text{eq}}_{\text{CS}}(x,\hat{k})}{4x(1-x)}, \quad (7)$$

where $S(\mathbf{k},\sigma) = \sum_j S_j e^{-i\mathbf{k}\cdot\mathbf{R}_j}$ is the structure factor and $\Delta E^{\text{eq}}_{\text{CS}}(x,\hat{k})$ is the constituent strain energy. It is defined as the energy change when the bulk solids A and B are deformed from their equilibrium cubic lattice constants a_A and a_B to a common lattice constant $a_\perp$ in the direction perpendicular to $\hat{k}$, while they are relaxed in the direction parallel to $\hat{k}$. It is given by

$$\Delta E^{\text{eq}}_{\text{CS}}(x,\hat{k}) = \min_{a_\perp} \left[(1-x)\Delta E^{\text{epi}}_{A}(a_\perp,\hat{k}) + x \Delta E^{\text{epi}}_{B}(a_\perp,\hat{k}) \right], \quad (8)$$

where $\Delta E^{\text{epi}}_{A}(a_\perp,\hat{k})$ is the strain energy required to deform A biaxially to $a_\perp$. The constituent strain energy corresponds to the $\mathbf{k} \to 0$ limit of $J_{\text{CS}}(x,\hat{k})$ and takes on different values depending on the direction in which this limit is taken. The nonanalyticity in $J_{\text{CS}}(x,\hat{k})$ as $\mathbf{k} \to 0$ corresponds to infinite-range real-space elastic interactions. Including these long-range terms explicitly (rather than trying to cluster expand them) removes the $\mathbf{k} \to 0$ nonanalyticity of $J_{\text{CS}}(x,\hat{k})$.

Numerical calculation of the constituent strain energy $\Delta E^{\text{eq}}_{\text{CS}}(x,\hat{k})$ is done in three steps. First, the epitaxial energies of each of the pure constituents are calculated. That is, for pure A and B, the total energies are calculated for several different values of $a_\perp$, while in each case, the unit cell is allowed to relax in the direction perpendicular to the interface to minimize the total energy. This series of energies, $\Delta E^{\text{eq}}_{A,B}(\hat{k},a_\perp)$, is then interpolated to all values of $a_\perp$ between a_A and a_B using a polynomial. This process is repeated for five principal directions of $\hat{k}$: (001), (011), (111), (201), and (311).

In the second step, $\Delta E^{\text{eq}}_{\text{CS}}(x,\hat{k})$ is determined by using the total epitaxial energy of $\Delta E^{\text{eq}}_{A}(\hat{k},a_\perp)$ and $\Delta E^{\text{eq}}_{B}(\hat{k},a_\perp)$ in Eq. (8), where the equilibrium in-plane lattice constant $a_\perp$, common to both A and B, is chosen to minimize the strain energy, and $\Delta E^{\text{epi}}(\hat{k},a_\perp) = E^{\text{epi}}(\hat{k},a_\perp) - E^{\text{epi}}(\hat{k},a_{\text{eq}})$. The constituent strain energy $\Delta E^{\text{eq}}_{\text{CS}}(x,\hat{k})$ is determined for arbitrary composition x and a finite number of directions $\hat{k}$. Figure 1 shows the constituent strain energy for V-Nb, V-Ta, and Nb-Ta alloys. Each of the energies $\Delta E^{\text{epi}}_{A}$ and $\Delta E^{\text{epi}}_{B}$ are positive definite by definition and, hence, the coherency strain must be positive definite. For V-Nb and V-Ta, the constituent strains are positive and anisotropic. For both the alloys, it is evident from Fig. 1 that all the curves are skewed to the V side. Figure 1 also shows that (111) is the softest and (100) is the hardest interface orientations. The constituent strain energy of the size-matched Nb-Ta alloy consists of positive as well as negative values for the different principal interface orientations $\hat{k}$ and is negligibly small in magnitude, which implies that as expected, the constituent strain contribution to the free energy is unimportant for size-matched alloys. Moreover, we made a comparison of the maximum of the elastic strain energy of V-Nb and V-Ta alloys with those of Mo-Ta, Cu-Au,

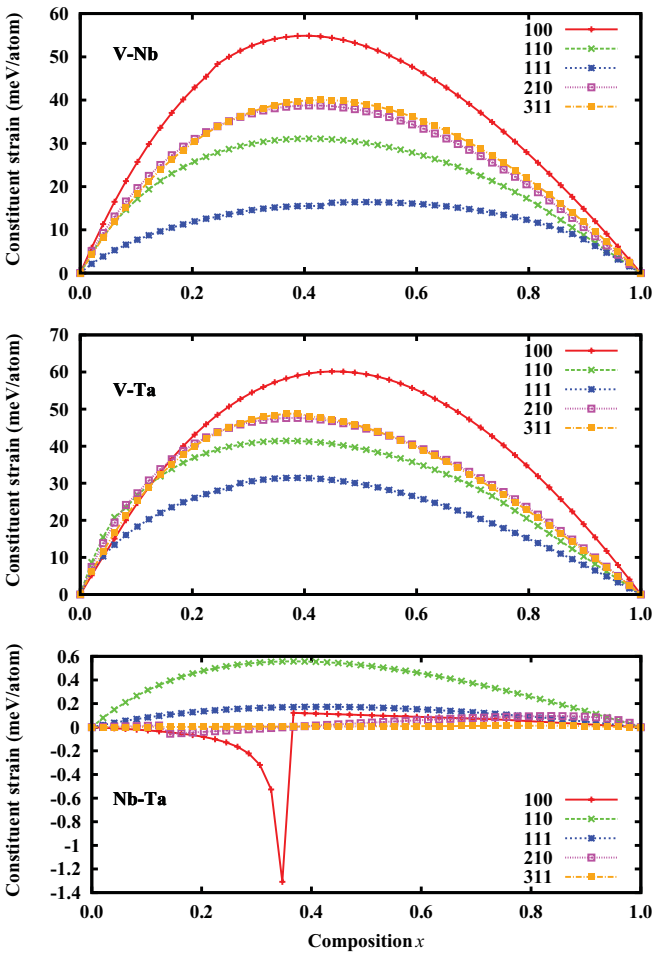

FIG. 1. (Color online) The constituent strain energy $\Delta E_{\mathrm{CS}}^{\mathrm{eq}}(x,\hat{k})$ of V-Nb, V-Ta, and Nb-Ta systems as a function of composition x for several principal interface orientations $\hat{k}$.

Cu-Ag, and Ni-Au alloys from the literature.[10,22,23] Figure 2 gives the comparison, which shows that the constituent strain energy scales with the magnitude of size mismatch of the alloy.

Finally, the constituent strain energy for arbitrary interface orientations $\hat{k}$ is interpolated by fitting the results obtained for the principal interface orientations to an expansion in Kubic harmonics:

$$\Delta E_{\mathrm{CS}}^{\mathrm{eq}}(x,\hat{k}) = \sum_{l=0}^{l_{\max}} c_l(x) K_l(\hat{k}). \tag{9}$$

Typically four or five terms are used in this expression as anharmonic effects are known to be significant.

D. Phonon entropy

The cluster expansion, including the constituent strain, described above, gives energies of arbitrary lattice configuration at 0 K and ignores the vibrational excitations. Early theoretical calculations of phase equilibrium have indicated that the phonon contribution should be included for improving the accuracy. Sanchez *et al.*,[58] in their study of the Ag-Cu alloy, have shown that even a crude model of the vibrational entropy

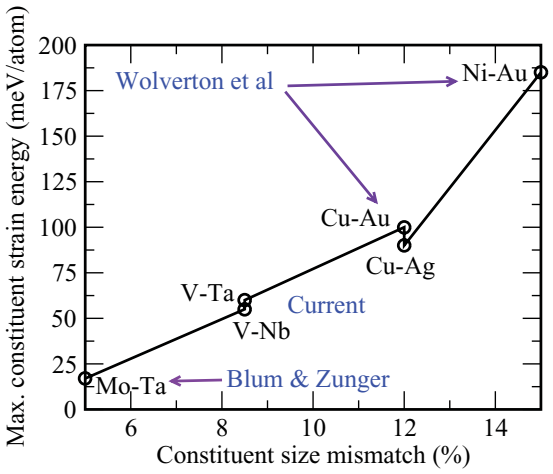

FIG. 2. (Color online) Comparison of the maximum of the constituent strain energy corresponding to principal interface orientations for V-Nb and V-Ta alloys with those of Mo-Ta, Cu-Au, Cu-Ag, and Ni-Au alloys from the literature (Refs. 10 and 22). The constituent strain energy scales with the magnitude of size mismatch of the alloy.

markedly improved the computed solubility with respect to the experimental data. Asta *et al.*,[19] in their work on the phase stability of the Cd-Mg system, have demonstrated that the nonconfigurational contributions to the free energy, such as phonon entropy, must be considered in any theoretical study of phase stability which hopes to obtain accurate results. In the case of Ni-Au alloys,[59] the nonconfigurational entropy of formation is shown to be essential to reconcile the experimental and theoretical miscibility gap temperatures. Recent first-principles theoretical studies[60–62] establish that the vibrational entropy contribution is indeed essential for accurate calculation of alloy phase equilibrium.

In a cluster expansion, a Hamiltonian for the alloy system is constructed by fitting the ground-state energies of typically 30–40 ordered configurations. Vibrational effects can be formally included by fitting to vibrational free energies, rather than ground-state energies. This requires computation of the force-constants tensor and phonon spectrum for the 30–40 structures, which is computationally expensive. On the other hand, first-principles calculation of phonon properties of Pd-V alloys has revealed that most of the variation in the stiffness of a given chemical bond across different structures can be explained by changes in the bond length.[28] Based on this, van de Walle and Ceder identified that the bond stiffness versus bond length relationship is transferable and showed that a linear relationship can be used as a first approximation.[29]

A scheme based on bond-length-dependent transferable force constants has been used successfully in several studies.[28,31,63,64] We use this scheme to compute the contribution of lattice vibrations to the free energy of V-Nb, V-Ta, and Nb-Ta alloys. This method proceeds by parametrizing the bond-length dependence of the stiffness for each type of nearest-neighbor chemical bond. This is achieved by calculating the reaction forces from various imposed atomic displacements away from their equilibrium positions, which is done for a few high-symmetry ordered supercells for a range

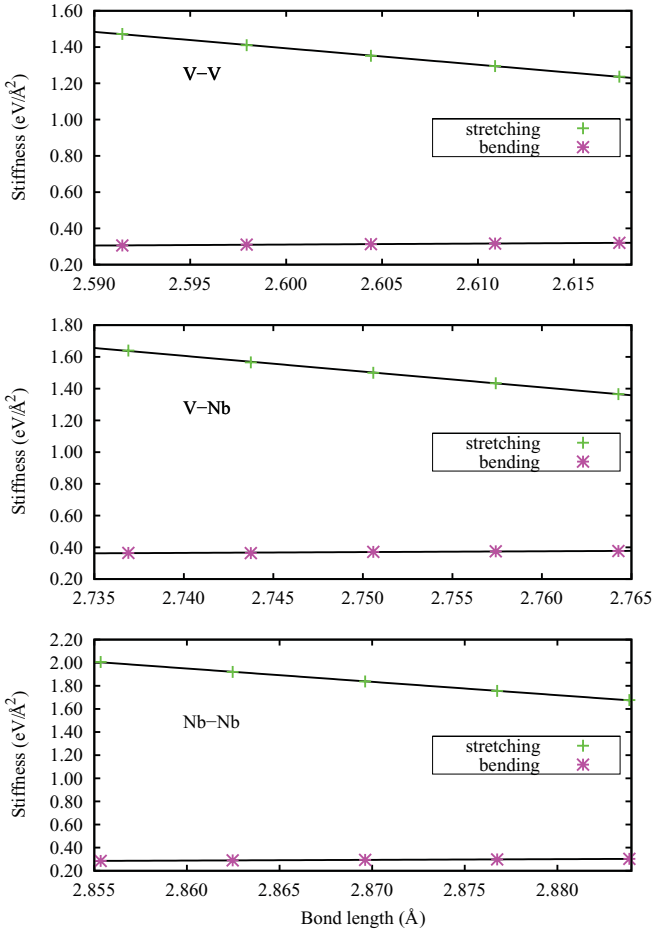

FIG. 3. (Color online) Nearest-neighbor bond stiffness (against stretching or bending) as a function of bond length for V-Nb alloys. Points indicate *ab initio* data and lines are linear fits representing the transferable force constants relation used in the calculations of the vibrational free energy.

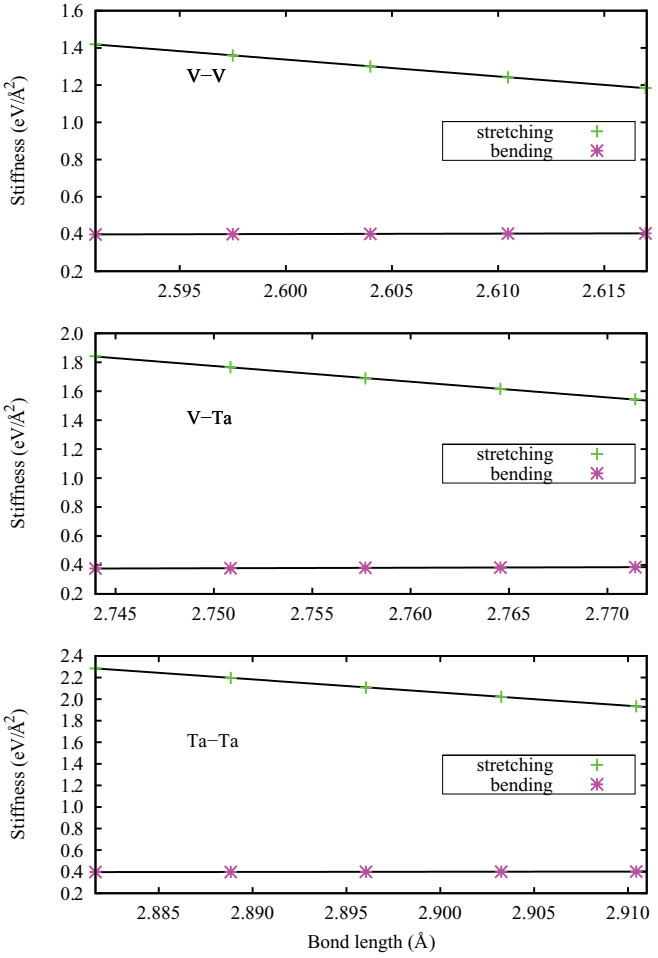

FIG. 4. (Color online) Nearest-neighbor bond stiffness as a function of bond length for V-Ta alloys. Points indicate *ab initio* data and lines are linear fits used in the calculations of the vibrational free energy.

of lattice parameters. In the present work, three structures, consisting of the two end members and a binary structure, were considered, for five values of the lattice parameter. The parameters defining the bond-length-dependent transferable force constants relation are then obtained from a polynomial fit of the calculated forces as a function of bond length. Figures 3–5 show that the linear relationship provides a reliable description of the nearest-neighbor force constants in V-Nb, V-Ta, and Nb-Ta alloys.

Once the bond-length dependence of bond stiffness is known, the nearest-neighbor inter-atomic force constants for any supercell configuration in the cluster expansion fit can be predicted from the relaxed bond lengths that are obtained from the VASP structure energy minimization. The standard lattice dynamics based on a nearest-neighbor bond Born–von Karman model[29,65] then provides the phonon density of states and, consequently, any thermodynamic property of interest, such as the vibrational contribution to the free energy. Configuration dependence of the vibrational free energy is parametrized with a cluster expansion with temperature-dependent effective cluster interactions.

E. Monte Carlo simulation

The free energies and phase boundaries of the alloys are calculated using Monte Carlo simulations in which the energetics of the system is specified by the cluster expansion Hamiltonian. The Monte Carlo simulations were performed using the program EMC2 of ATAT, which is described elsewhere.[66] EMC2 samples a semi-grand-canonical ensemble in which the chemical potential, $\Delta\mu$, and the temperature, T, are specified with a conserved total number M $(=\sum_{i=1}^{c} M_i)$ of particles. The composition $x \equiv \{\frac{M_i}{M}; i = 2, \ldots, c\}$ is allowed to vary with a constraint of fixed $\sum_{i=1}^{c} M_i = M$. The method of thermodynamic integration is used to determine the grand canonical potential ϕ^{α} of each phase α as a function of $\Delta\mu$. The grand canonical potential at the starting point of the integration path is obtained from the high- or low-temperature series expansion. We have used a $34 \times 34 \times 34$ supercell for the direct Monte Carlo simulations and a $8 \times 8 \times 8$ supercell for the k-space Monte Carlo simulations involving constituent strains. The EMC2 program automatically determines the equilibration and the averaging times for the given precision on the average concentration of the alloy, which was set to $\leqslant 0.1\%$ in the current simulations.

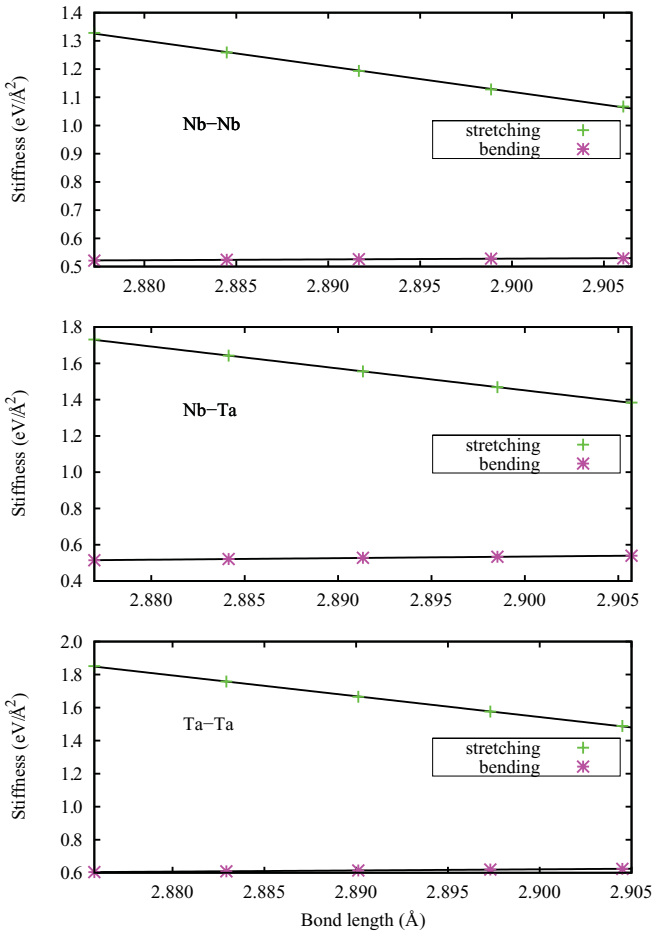

FIG. 5. (Color online) Nearest-neighbor bond stiffness as a function of bond length for Nb-Ta alloys. Points indicate *ab initio* data and lines are linear fits used in the calculations of the vibrational free energy.

III. RESULTS

A. Effective cluster interactions and ground-state structures

1. V-Nb alloys

The effective cluster interactions (ECIs) of V-Nb alloy are shown in Fig. 6. ECIs shown in Fig. 6(a) are solely characteristic of chemical interaction and their configuration dependence. Figure 6(b) shows ECIs which include the constituent strain interaction in addition to chemical interaction. Both sets of ECIs show approximately the same pattern except that the set of ECIs which includes the constituent strain contains a three-body interaction parameter in place of a pair interaction parameter of the set of ECIs which neglects the constituent strain. We see that the first- and second-neighbor pair interaction parameters are negative, which is related to the tendency to phase separate.[10,67] While the first- and second-neighbor pair ECIs constitute the dominant interactions, it is evident that the second-neighbor pair interaction is more than twice stronger than the nearest-neighbor pair interaction. A similar pattern of interactions is seen in the previous studies of Ni-Au and Ni-Pt alloys.[37,59]

Figure 7(a) shows the energy of formation, $\Delta H_{\mathrm{CE}}(\sigma)$, versus the concentration of all bcc supercells containing

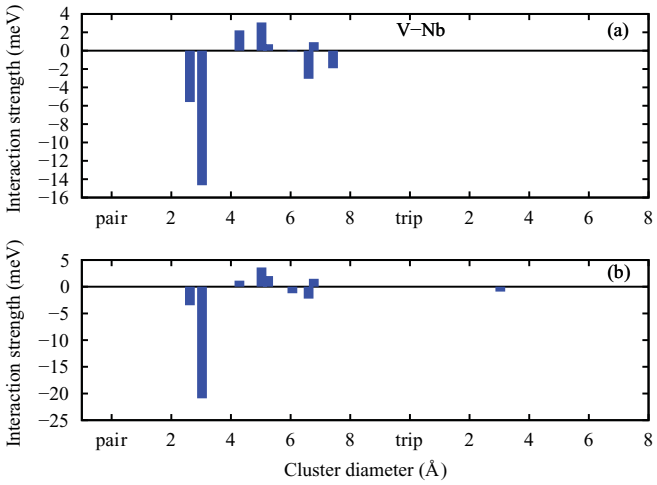

FIG. 6. (Color online) Effective cluster interactions of V-Nb alloys. (a) is characteristic solely of configuration-dependent chemical interactions. (b) represents cluster expansion that includes both the chemical and constituent strain interactions.

up to 12 atoms, predicted using the interactions shown in Fig. 6. The direct enumeration approach[35] has been used for constructing the ground-state hull. The ground states are identified as breaking points of the concentration versus energy of formation convex hull. For an equiatomic V-Nb alloy, our cluster expansion predict that the lowest energy of formation is 20 meV/atom, which is in agreement with the (23 meV/atom) CALPHAD energy of formation of the bcc solid solution.[68] Figure 7(b) depicts the ground-state search after the constituent strain is included. The constituent strain has only shifted the ground-state line slightly. Moreover, in agreement with the experimental absence of long-range ordered phases, the current cluster expansion does not predict any intermediate ground states.

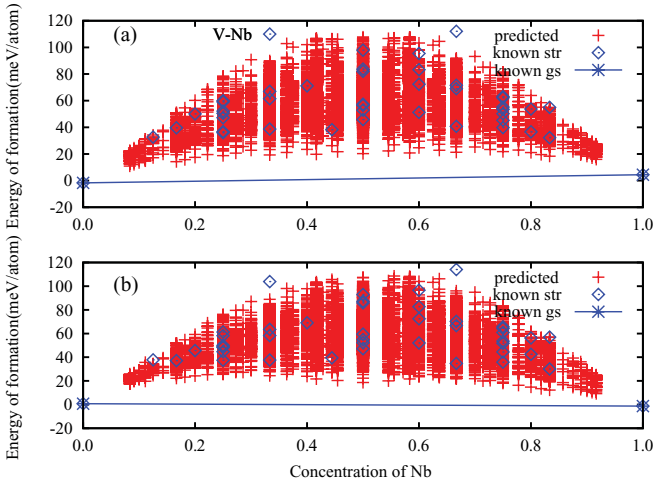

FIG. 7. (Color online) Ground-state search of V-Nb alloys covering all bcc supercells containing up to 12 atoms. (a) is obtained with conventional cluster expansion. (b) is obtained with a Hamiltonian that includes the constituent strain interactions.

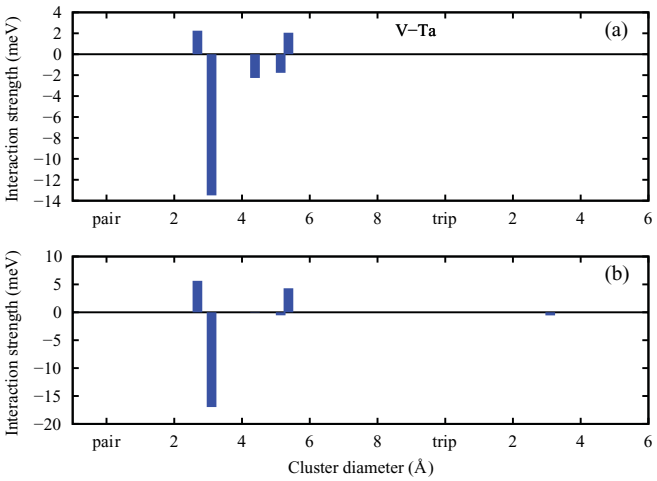

FIG. 8. (Color online) Effective cluster interactions of the V-Ta alloys. (a) is characteristic solely of configuration-dependent chemical interactions. (b) represents cluster expansion that includes both the chemical and constituent strain interactions.

2. V-Ta alloys

The effective cluster interactions of bcc V-Ta alloy are shown in Fig. 8. The ECIs shown in Fig. 8(a) are characteristic of chemical interaction only. Figure 8(b) shows the ECIs representing both the chemical and constituent strain interactions. It is evident that the constituent strain has additionally introduced a three-body interaction, besides a set of five pair interactions. The nearest-neighbor pair interaction is positive, which is related to ordering tendency.[10,67] The dominant negative second-neighbor pair interaction, however, appears to counteract with the ordering tendency. Figure 9(a) shows the $\Delta H_{\mathrm{CE}}(\sigma)$ versus the concentration of all bcc supercells containing up to 12 atoms. For an equiatomic V-Ta alloy, our cluster expansion predicts that the energy of formation is 17 meV/atom, which is comparable to the CALPHAD value

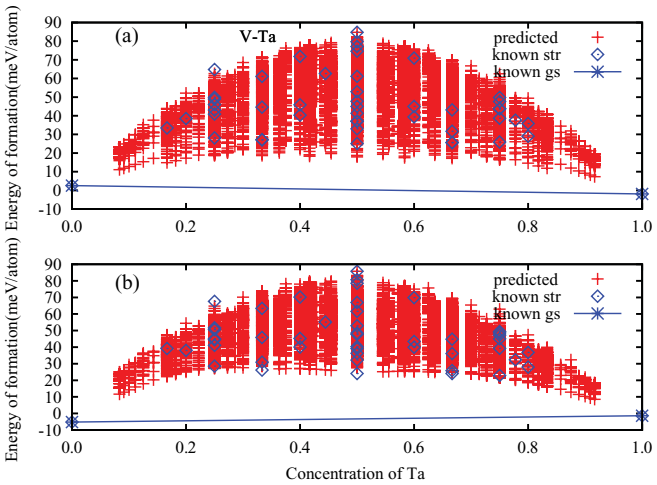

FIG. 9. (Color online) Ground-state search of V-Ta alloys covering all bcc supercells containing up to 12 atoms. (a) is obtained with conventional cluster expansion. (b) is obtained with a Hamiltonian that includes the constituent strain to the conventional cluster expansion.

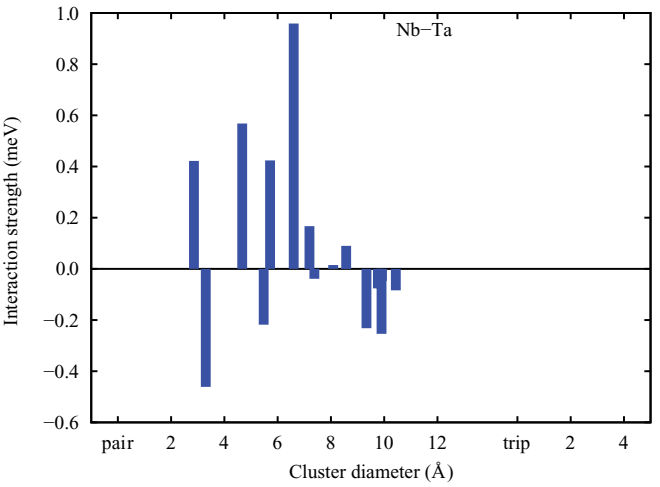

FIG. 10. (Color online) Effective cluster interactions of the Nb-Ta alloys.

of 12 meV/atom of the solution phase.[69] Figure 9(b) shows the result of ground-state search after the constituent strain is included. The constituent strain has shifted the ground-state line slightly, without predicting any new ground states. We note that the current cluster expansion assumes a bcc Bravais lattice for the alloy and consider only bcc super structures, ignoring the V_2Ta Laves phase.

3. Nb-Ta alloys

The effective cluster interactions of Nb-Ta alloy are shown in Fig. 10. Nb-Ta is a size-matched alloy. The Nb-Ta cluster expansion includes many distant neighbor pair interactions. However, the strengths of these interactions are an order of magnitude smaller compared to that in V-Nb and V-Ta alloys. Figure 11 shows the $\Delta H_{\mathrm{CE}}(\sigma)$ versus the concentration ground-state search for all bcc supercells containing up to 12 atoms. It is evident that the cluster expansion has predicted several intermediate ground states. The formation enthalpy of these ground-states are, however, very small, less than −8 meV/atom. This indicates that the ordering temperatures

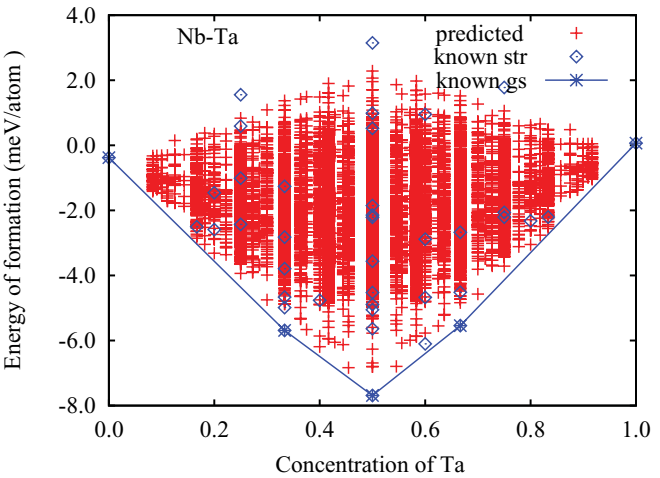

FIG. 11. (Color online) Ground-state search of Nb-Ta alloys covering all bcc supercells containing up to 12 atoms.

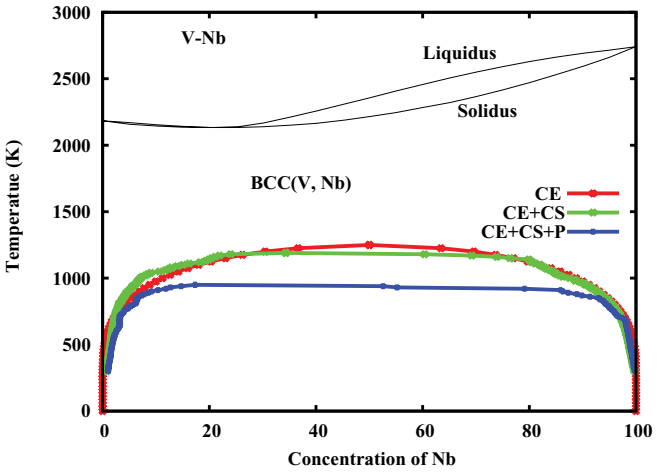

FIG. 12. (Color online) The calculated phase diagram of V-Nb alloys compared with experiments. The liquidus and solidus are the experimental phase boundaries (Ref. 9). The curves with label CE represent results of the conventional cluster expansion. CS and P represent results obtained by adding the constituent strain and phonon contributions, respectively. The conventional cluster expansion predicts an appreciable miscibility gap. The phonon contribution lowers the miscibility gap temperature by about 24%.

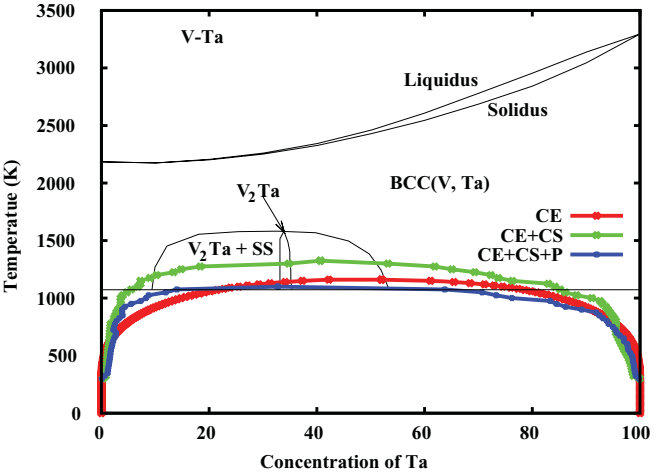

FIG. 13. (Color online) The calculated phase diagram of V-Ta alloys compared with experiments. The solidus, liquidus, and phase boundaries associated with the V_2Ta are the experimental phase boundaries (Ref. 9). The curves with label CE represent the results of conventional cluster expansion. CS and P represent the results obtained by adding the constituent strain and phonon contributions, respectively. The horizontal line at 1073 K is incorporated to indicate that the experimental phase diagram is not available below 1073 K.

for these phases will be very low[70] and therefore cannot be readily observed in the experiments.

B. Phase diagrams

1. V-Nb alloys

The phase diagram of V-Nb alloys, obtained by thermodynamic modeling of the experimental data, exhibit a continuous series of solid solutions. X-ray diffraction patterns of several alloys in the composition range 20–50 at. % Nb, with long-term annealing (113 hours at 923 K and 170 hours at 1173 K), did not show any phase other than the bcc solid solution. Melting point as well as the cooling curve determination have also not shown any solid-state phase transformations.[8,9]

The computed phase diagram of V-Nb alloys is compared with the so-called experimental results in Fig. 12. The phase boundary with label CE represents the result of the conventional cluster expansion, which considers only chemical interactions. The labels CS and P represent the results obtained by adding the constituent strain and phonon contributions, respectively. It is evident that the conventional cluster expansion predicts a miscibility gap with a consolute temperature (the critical temperature above which the components of a mixture are miscible in all proportions) $T_c = 1250$ K. The constituent strain does not change the miscibility gap temperature appreciably, although it appears to alter the solubility of V- and Nb-rich alloys. The phonon contribution, combined with the constituent strain, has lowered the miscibility gap temperature significantly to 950 K (about 24%). Our calculations thus predict an appreciable miscibility gap for V-Nb alloys.

2. V-Ta alloys

The V-Ta phase diagram obtained by assessing the experimental thermodynamic data exhibits complete miscibility in the solid state above 1583 K. Below this, the phase diagram consists of a major solid solution region and a two-phase region made up of the bcc V-Ta solution and the V_2Ta fcc Laves phase.[9,69] The experimental phase diagram is not available below 1073 K, although CALPHAD models exist. The current V-Ta phase diagram calculation uses a cluster expansion based on bcc lattice and ignores the V_2Ta phase. Figure 13 compares the calculated phase boundaries with experiments. The phase boundary with label CE represents the result of the conventional cluster expansion. The labels CS and P represent the result of adding the constituent strain and phonon contributions. The phase boundary computed with the conventional cluster expansion shows that the V-Ta is completely miscible above 1160 K and phase separates below this temperature. When the constituent strain is included, the miscibility gap temperature is increased to 1325 K (about 12%). This shows that the constituent strain is significant in V-Ta alloys compared to V-Nb alloys. When the phonon contribution is also included, the miscibility gap temperature is lowered to 1100 K. This indicates that the constituent strain and phonon interactions have competing effects on the phase transition temperature of V-Ta alloys. Moreover, we have seen that the constituent strain energy, for high-symmetry interface orientations, is slightly higher for V-Ta compared to V-Nb alloys. The influence of the constituent strain energy on the phase transition temperature is found to be correspondingly more appreciable in V-Ta alloys than in V-Nb alloys.

3. Nb-Ta alloys

The Nb-Ta phase diagram, obtained by thermodynamic modeling of the experimental data, shows complete miscibility in the solid state without any evidence of a solid-state phase transformation.[9] Figure 14 shows the computed phase boundary, which almost lies on the horizontal axis. This phase

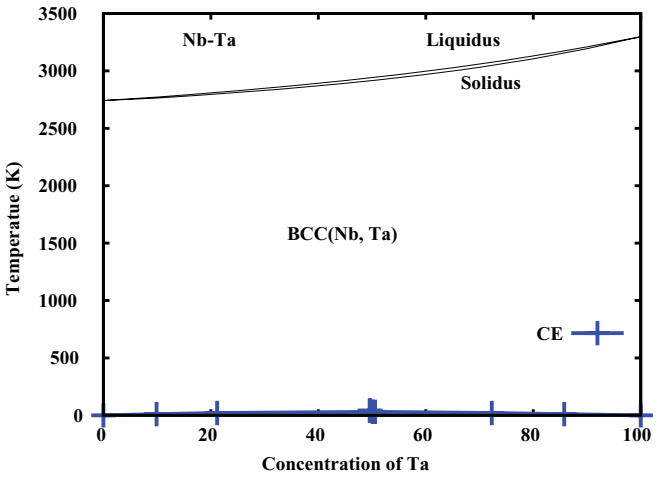

FIG. 14. (Color online) The calculated phase diagram of size-matched Nb-Ta alloys compared with experiments. The solidus and liquidus are experimental phase boundaries. The computed phase boundary, with label CE, lies almost on the horizontal axis indicating complete miscibility down to 40 K.

boundary is obtained with the conventional cluster expansion. The phonon contribution was found to have no appreciable effect on the phase boundary. The constituent strain is ignored as it vanishes in size-matched alloys. This calculation thus predicts complete miscibility of Nb and Ta and the solution phase is stable down to 40 K in agreement with experiment.

IV. DISCUSSION

The chemical and the constituent strain interactions are the two key factors governing ordering or phase-separation behavior of an alloy. The chemical interactions give attractive contribution to the free energy of formation. The constituent strain gives a repulsive contribution. The vibrational entropy captures the variation in the phonon properties associated with alloying which alters the stiffness of the chemical bonds. According to the experiments, V-Nb forms a solid solution without a miscibility gap. On the other hand, our calculations predict an appreciable miscibility gap with $T_c = 950$ K. Our cluster expansion covers all bcc supercells containing up to 12 atoms. Including structures with more atoms per unit cell would modify the ECIs. Furthermore, the transferable force constants scheme of lattice dynamics calculation is approximate. These factors are likely to influence the computed phase boundaries. On the other hand, generally, in high-melting alloys, the slow atomic diffusion at low temperatures often prevents direct observation of either phase separation or ordering, and only the high-temperature disordered solid-state behavior is observed. Therefore, it is likely that miscibility gap predicted by our first-principles calculations is overlooked in the experiments due to slow kinetics.

The solid-state part of the V-Ta experimental phase diagram consists mainly of two regions: (i) a bcc V-Ta solution region and (ii) a two-phase region made up of V_2Ta and the solution phase. Table I gives the physical properties and ground-state structures of V-Nb, V-Ta, and Nb-Ta alloys. V-Nb and V-Ta alloys have nearly the same size mismatch. This indicates that both the alloys should have same the constituent strain

TABLE I. Physical properties and ground-state structures of V-Nb, V-Ta, and Nb-Ta alloys. Given are constituent size mismatches $\Delta a/\bar{a} = 2(a_A - a_B)/(a_A + a_B)$, electronegativity difference on the Pauling scale $\Delta\chi$, and low-temperature phases.

System	$\Delta a/\bar{a}$	$\Delta\chi$	Low-Temperature Phases
V-Nb	8.54%	0.03	Solid solution
V-Ta	8.57%	0.13	V_2Ta and solid solution
Nb-Ta	0.03%	0.10	Solid solution

energies. On the other hand, the electronegativity difference of V-Ta is significantly higher compared to that of V-Nb. Electronegativity difference often controls the charge transfer and hence the bonding. This means that, due to the large electronegativity difference, chemical interactions dominate in V-Ta alloys which leads to the ordering transition at 1583 K with the formation of the V_2Ta phase from the solution phase.

Our calculation for V-Ta alloys, which ignores the V_2Ta phase, predicts a miscibility gap with consolute temperature $T_c = 1100$ K, which is appreciably lower than 1583 K. Formation of the V_2Ta phase is driven by the dominant chemical interaction in the alloy, which appears to manifest by making the solution phase remain stable down to 1100 K.

V. SUMMARY AND CONCLUSION

We have computed the phase equilibrium of V-Nb, V-Ta, and Nb-Ta alloys by combining density functional theory total energy calculations with the cluster expansion and Monte Carlo techniques. For V-Nb alloys, the phase boundary computed with the conventional cluster expansion produces a miscibility gap with a consolute temperature $T_c = 1250$ K. Including the constituent strain to the cluster expansion Hamiltonian does not alter the miscibility gap significantly, although it appears to influence the solubility of V- and Nb-rich alloys. The phonon entropy, combined with the constituent strain, lowers the miscibility gap temperature significantly to 950 K. The predicted miscibility gap of V-Nb alloys is appreciable compared to the complete miscibility claimed by the experiments. While the accuracy of the cluster expansion can be improved by considering structures with more atoms and better lattice dynamics models, it is also likely that, in the alloys with high-melting point, the slow atomic diffusion at low temperature prevented observation of phase separation or ordering. For bcc V-Ta alloys, this calculation predicts a miscibility gap with $T_c = 1100$ K. For these alloys, both the constituent strain and phonon contributions are found to be significant. The constituent strain increases the miscibility gap while phonon entropy reverses the effect of the constituent strain. In V-Ta alloy, the ordering transition occurs at 1583 K from bcc solid solution to the V_2Ta Laves phase due to the dominant chemical interaction associated with the relatively large electronegativity difference. Since the current cluster expansion ignores the V_2Ta phase, the associated chemical interaction appears to manifest in making the solid solution phase remain stable down to 1100 K. For Nb-Ta alloys, our calculation predicts complete miscibility in agreement with experiment.

*ravic@igcar.gov.in

[1] M. Ishizuka, M. Iketani, and S. Endo, Phys. Rev. B **61**, R3823 (2000).

[2] F. A. Khwaja and F. Brouers, Phys. Status Solidi B **139**, 565 (1987).

[3] A. Landa, P. Soderlind, A. V. Ruban, O. E. Peil, and L. Vitos, Phys. Rev. Lett. **103**, 235501 (2009).

[4] A. Landa, P. Soderlind, O. I. Velikokhatnyi, I. I. Naumov, A. V. Ruban, O. E. Peil, and L. Vitos, Phys. Rev. B **82**, 144114 (2010).

[5] R. K. Bollinger, B. D. White, J. J. Neumeier, H. R. Z. Sandim, Y. Suzuki, C. A. M. dos Santos, R. Avci, A. Migliori, and J. B. Betts, Phys. Rev. Lett. **107**, 075503 (2011).

[6] V. V. Shyrokov, Ch. B. Vasyliv, and O. V. Shyrokov, J. Nucl. Mater. **394**, 114 (2009).

[7] M. Muzyk, D. Nguyen-Manh, K. J. Kurzydlowski, N. L. Baluc, and S. L. Dudarev, Phys. Rev. B **84**, 104115 (2011).

[8] A. E. Vol, *Handbook of Binary Metallic Systems: Structure and Properties* (translated from the Russian by the Israel Program for Scientific Translation Ltd., Jerusalem, 1967), Vol. II, p. 813.

[9] *Binary Alloy Phase Diagrams*, edited by T. B. Massalski, Hiroaki Okamoto, P. R. Subramanian, and Lind Kacprzak (ASM International, Materials Park, OH, 1990), Vol. 3.

[10] V. Blum and A. Zunger, Phys. Rev. B **70**, 155108 (2004).

[11] Y. Z. Shen, S. H. Kim, C. H. Han, H. D. Cho, W. S. Ryu, and C. B. Lee, J. Nucl. Mater. **374**, 403 (2008).

[12] F. Abe, Sci. Technol. Adv. Mater. **9**, 013002 (2008).

[13] M. Albu, F. Méndez Martin, G. Kothleitner, and B. Sonderegger, Int. J. Mat. Res. **4**, 422 (2008).

[14] M. Tamura, M. Nakamura, K. Shinozuka, and H. Esaka, Metall. Mater. Trans. A **39**, 1060 (2008).

[15] P. Lazar, R. Podloucky, E. Kozeschnik, and J. Redinger, Phys. Rev. B **78**, 134202 (2008).

[16] H. Magnusson and R. Sandstrom, Mater. Sci. Eng. A **527**, 118 (2009).

[17] L. G. Ferreira, A. A. Mbaye, and A. Zunger, Phys. Rev. B **37**, 10547 (1988).

[18] D. B. Laks, L. G. Ferreira, S. Froyen, and A. Zunger, Phys. Rev. B **46**, 12587 (1992).

[19] M. Asta, R. McCormack, and D. de Fontaine, Phys. Rev. B **48**, 748 (1993).

[20] A. Zunger, in *Statics and Dynamics of Alloy Phase Transformations*, edited by P. E. A. Turchi and A. Gonis (Plenum Press, New York, 1994), p. 361.

[21] Z. W. Lu, D. B. Laks, S.-H. Wei, and A. Zunger, Phys. Rev. B **50**, 6642 (1994).

[22] C. Wolverton, V. Ozolins, and A. Zunger, Phys. Rev. B **57**, 4332 (1998).

[23] V. Ozolins, C. Wolverton, and A. Zunger, Phys. Rev. B **57**, 4816 (1998).

[24] V. Ozolins, C. Wolverton, and A. Zunger, Phys. Rev. B **57**, 6427 (1998).

[25] S. Muller, L.-W. Wang, A. Zunger, and C. Wolverton, Phys. Rev. B **60**, 16448 (1999).

[26] G. Ceder, Comput. Mater. Sci. **1**, 144 (1993).

[27] G. D. Garbulsky and G. Ceder, Phys. Rev. B **49**, 6327 (1994).

[28] A. van de Walle and G. Ceder, Phys. Rev. B **61**, 5972 (2000).

[29] A. van de Walle and G. Ceder, Rev. Mod. Phys. **74**, 11 (2002).

[30] E. J. Wu, G. Ceder, and A. van de Walle, Phys. Rev. B **67**, 134103 (2003).

[31] B. P. Burton and A. van de Walle, Chemical Geology **225**, 222 (2006).

[32] J. Z. Liu, G. Ghosh, A. van de Walle, and M. Asta, Phys. Rev. B **75**, 104117 (2007).

[33] J. M. Sanchez, F. Ducastelle, and D. Gratias, Physica A **128**, 334 (1984).

[34] Z. W. Lu, S.-H. Wei, A. Zunger, S. Frota-Pessoa, and L. G. Ferreira, Phys. Rev. B **44**, 512 (1991).

[35] L. G. Ferreira, S.-H. Wei, and A. Zunger, Int. J. Supercomp. Appl. **5**, 34 (1991).

[36] C. Wolverton and A. Zunger, Phys. Rev. B **50**, 10548 (1994).

[37] A. Zunger, L. G. Wang, G. L. W. Hart, and M. Sanati, Modell. Simul. Mater. Sci. Eng. **10**, 685 (2002).

[38] J. M. Sanchez, Phys. Rev. B **81**, 224202 (2010).

[39] C. Ravi, H. K. Sahu, M. C. Valsakumar, and A. van de Walle, Phys. Rev. B **81**, 104111 (2010).

[40] J. W. D. Connolly and A. R. Williams, Phys. Rev. B **27**, 5169 (1983).

[41] G. Kresse and J. Hafner, Phys. Rev. B **47**, 558 (1993).

[42] G. Kresse and J. Furthmuller, Phys. Rev. B **54**, 11169 (1996).

[43] Y. Wang and J. P. Perdew, Phys. Rev. B **44**, 13298 (1991).

[44] J. P. Perdew and Y. Wang, Phys. Rev. B **45**, 13244 (1992).

[45] J. P. Perdew, J. A. Chevary, S. H. Vosko, K. A. Jackson, M. R. Pederson, D. J. Singh, and C. Fiolhais, Phys. Rev. B **46**, 6671 (1992).

[46] J. P. Perdew, in *Electronic Structure of Solids'91*, edited by P. Ziesche and H. Eschrig (Akademie Verlag, Berlin, 1991).

[47] P. E. Blochl, Phys. Rev. B **50**, 17953 (1994).

[48] G. Kresse and D. Joubert, Phys. Rev. B **59**, 1758 (1999).

[49] M. Methfessel and A. T. Paxton, Phys. Rev. B **40**, 3616 (1989).

[50] H. J. Monkhorst and J. D. Pack, Phys. Rev. B **13**, 5188 (1976).

[51] A. van de Walle and G. Ceder, J. Phase Equilib. **23**, 348 (2002).

[52] A. van de Walle, Calphad **33**, 266 (2009).

[53] ATAT manual, [http://www.its.caltech.edu/∼avdw/atat].

[54] S. Muller, C. Wolverton, L.-W. Wang, and A. Zunger, Acta Mater. **48**, 4007 (2000).

[55] C. Wolverton, Modell. Simul. Mater. Sci. Eng. **8**, 323 (2000).

[56] C. Wolverton, V. Ozolins, and A. Zunger, J. Phys. Condens. Matter **12**, 2749 (2000).

[57] S. Muller, J. Phys. Condens. Matter **15**, R1429 (2003).

[58] J. M. Sanchez, J. P. Stark, and V. L. Moruzzi, Phys. Rev. B **44**, 5411 (1991).

[59] C. Wolverton and A. Zunger, Comput. Mater. Sci. **8**, 107 (1997).

[60] C. Ravi, C. Wolverton, and V. Ozolins, Europhys. Lett. **73**, 719 (2006).

[61] V. Ozolins and M. Asta, Phys. Rev. Lett. **86**, 448 (2001).

[62] C. Wolverton and V. Ozolins, Phys. Rev. Lett. **86**, 5518 (2001).

[63] O. Adjaoud, G. Steinle-Neumann, B. P. Burton, and A. van de Walle, Phys. Rev. B **80**, 134112 (2009).

[64] P. Dalach, D. E. Ellis, and A. van de Walle, Phys. Rev. B **82**, 144117 (2010).

[65] A. A. Maradudin, E. W. Montroll, and G. H. Weiss, *Theory of Lattice Dynamics in Harmonic Approximation*, 2nd ed. (Academic Press, New York, 1971).

[66] A. van de Walle and M. Asta, Modell. Simul. Mater. Sci. Eng. **10**, 521 (2002).

[67] V. Blum and A. Zunger, Phys. Rev. B **72**, 020104 (2005).

[68] K. C. Hari Kumar, P. Wollants, and L. Delaey, Calphad **18**, 71 (1994).

[69] C. A. Danon and C. Servant, J. Alloys Compd. **366**, 191 (2004).

[70] B. Kolb, S. Muller, D. B. Botts, and G. L. W. Hart, Phys. Rev. **74**, 144206 (2006).